Modulated photophysics of a cationic DNA-staining dye inside protein bovine serum albumin: study of binding interaction and structural changes of protein. Spectrochim Acta A Mol Bi...

ARTICLE *in* SPECTROCHIMICA ACTA PART A MOLECULAR AND BIOMOLECULAR SPECTROSCOPY · OCTOBER 2013

Impact Factor: 2.35 · DOI: 10.1016/j.saa.2013.10.049 · Source: PubMed

4 AUTHORS, INCLUDING:

Sankar Jana
Tohoku University
33 PUBLICATIONS **352** CITATIONS

SEE PROFILE

Spectrochimica Acta Part A: Molecular and Biomolecular Spectroscopy 121 (2014) 23–34

Contents lists available at ScienceDirect

Spectrochimica Acta Part A: Molecular and Biomolecular Spectroscopy

journal homepage: www.elsevier.com/locate/saa

Modulated photophysics of a cationic DNA-staining dye inside protein bovine serum albumin: Study of binding interaction and structural changes of protein

Anuva Samanta, Sankar Jana, Debarati Ray, Nikhil Guchhait *

Department of Chemistry, University of Calcutta, 92, A.P.C. Road, Kolkata 700009, India

HIGHLIGHTS

- Binding interaction of DNA intercalating dye PI with BSA.
- Quenching of BSA by PI is static in nature.
- Binding of PI occur in Sudlow site I of BSA.
- Hydrophobic interaction plays the main role in this probe–protein interaction.

GRAPHICAL ABSTRACT

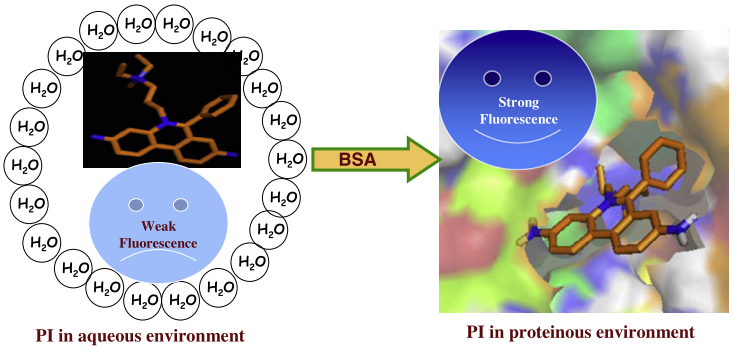

ARTICLE INFO

Article history:
Received 28 August 2013
Received in revised form 1 October 2013
Accepted 9 October 2013
Available online 20 October 2013

Keywords:
Bovine serum albumin
Propidium iodide
Fluorescence resonance energy transfer
Site marker
Circular dichroism
Chemical denaturation

ABSTRACT

The binding affinity of cationic DNA-staining dye, propidium iodide, with transport protein, bovine serum albumin, has been explored using UV–vis absorption, fluorescence, and circular dichroism spectroscopy. Steady state and time resolved fluorescence studies authenticate that fluorescence quenching of bovine serum albumin by propidium iodide is due to bovine serum albumin–propidium iodide complex formation. Thermodynamic parameters obtained from temperature dependent spectral studies cast light on binding interaction between the probe and protein. Site marker competitive binding has been encountered using phenylbutazone and flufenamic acid for site I and site II, respectively. Energy transfer efficiency and distance between bovine serum albumin and propidium iodide have been determined using Förster mechanism. Structural stabilization or destabilization of protein by propidium iodide has been investigated by urea denaturation study. The circular dichroism study as well as FT-IR measurement demonstrates some configurational changes of the protein in presence of the dye. Docking studies support the experimental data thereby reinforcing the binding site of the probe to the subdomain IIA of bovine serum albumin.

Introduction

Propidium iodide (PI), chemically 3-(3,8-diamino-6-phenyl-6H-phenanthridin-5-yl)propyl-diethyl-methylazanium, derivative of ethidium ion, is well known and widely used as intercalating dye due to its striking fluorescence enhancement upon binding with DNA [1–3]. PI interacts with different nucleic acids through intercalation between the bases with little or no specific sequence preference and has been studied recently [4]. Krishan, in a simpler and quicker staining method, has described the use of PI as a fluorescent DNA intercalating label for the analysis of DNA per cell by flow cytometry [5]. It can also be used to differentiate necrotic, apoptotic and normal cells [6]. A typical use of PI is the evaluation

* Corresponding author. Tel.: +91 33 2350 8386; fax: +91 33 2351 9755.
E-mail address: nguchhait@yahoo.com (N. Guchhait).

1386-1425/$ - see front matter © 2013 Elsevier B.V. All rights reserved.
http://dx.doi.org/10.1016/j.saa.2013.10.049

of cell death and apoptosis or determination of DNA content in the cell cycle analysis [7]. PI is also useful in estimating the proportion of living and dead sperm in a variety of mammals [3]. In spite of broad uses of propidium iodide, the interaction mechanism between PI and protein and the impact of PI on the conformation of protein are still not explored. In the pharmaceutical industry, it is widely authenticated that the overall distribution and efficacy of many drugs can be modified based on their affinity to protein serum albumin [8–10]. In this article, efforts have been given to study the binding interaction of PI with BSA in details for an understanding of the mechanism of the various classes of pharmaceutical interactions with serum albumin that can recommend new approaches to drug therapy and design.

Serum albumin, often referred to simply albumin, is the most prominent protein in blood plasma which carries a wide variety of endogeneous and exogeneous compounds including fatty acids, amino acids, bile salts, metals, hormones, drugs, chemical contaminants and pharmaceuticals [11–18]. Various researchers have reported the structural aspects and properties of these transport protein [19–21]. The crystal structure of bovine serum albumin (BSA) and human serum albumin (HSA) has already been resolved [22]. Here, BSA has been chosen as our model protein because of its medical importance, ready availability, and unusual ligand-binding properties and especially due to its structural homology with HSA. In fact, BSA and HSA are homologous protein and the tertiary structure of BSA is about 76% similar to that of HSA [23]. BSA is a large globular protein (66,000Dal) consisting of a single chain of 583 amino acids residues. It is made up of three homologous domains I, II and III which are divided into nine loops connected by 17 disulphide bonds. Each domain in turn is the product of two subdomains like IA, and IB [24]. BSA has two tryptophan residues that possess intrinsic fluorescence. Trp-213 locates within a hydrophobic binding pocket in the subdomain IIA, and Trp-134 locates on the surface of the albumin molecule in domain I [25]. For the study of structural and dynamical information of protein cavities and the binding interaction of foreign species, steady state and time-resolved fluorescence spectroscopy have attracted much attention for many research groups [26–30]. In the present work, we have explored a spectroscopic analysis on the influence of a cationic dye PI to monitor the conformational changes of protein in absence and presence of chaotropes. The quenching of the intrinsic tryptophanyl fluorescence of BSA has also been used as a tool to study the interaction of PI with this transport protein and to characterize any conformational change of protein. Meanwhile, several measurements including fluorescence quenching, synchronous and 3D-fluorescence spectra, CD and FT-IR measurements have been employed to achieve the binding constants, thermodynamic parameters and the structural changes of BSA. Site selective binding of the probe with protein has also been explored here with site markers. Protein–probe docking studies have been employed to find the probable location of the probe molecule bound to the protein environment.

Materials and methods

Reagents

Propidium iodide (Scheme 1) from Sigma–Aldrich was used as received without further purification. BSA and urea were purchased from SRL, India. Tris–HCl buffer (0.01 M, pH = 7.0) was prepared from Tris–HCl buffer purchased from SRL, India. Triple distilled water was used for the preparation of buffer solution. Site markers, Phenylbutazone and flufenamic acid, were obtained from Lancaster and Fluka, respectively. BSA concentrations were determined by UV–vis absorption measurements at 280 nm using $\varepsilon = 36{,}500\ M^{-1}\ cm^{-1}$ [31].

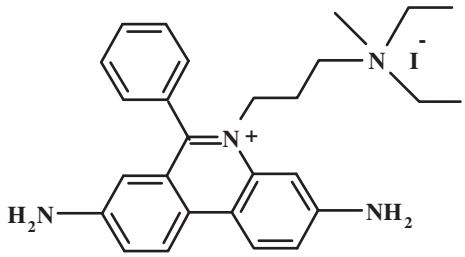

Scheme 1. Structure of propidium iodide.

Fluorescence and UV–vis absorption

The room temperature absorption and fluorescence spectra were recorded using Hitachi UV–vis U-3501 spectrophotometer and PerkinElmer LS-55 fluorimeter, respectively. Synchronous fluorescence spectra were recorded with $\Delta\lambda$ value between the excitation and emission wavelength fixed at 15 nm and 60 nm, respectively. The 3D-fluorescence spectra were performed maintaining the following conditions: the emission wavelength was recorded between 200 and 500 nm. The initial excitation wavelength was set to 200 nm with increment of 5 nm and 30 scan. Steady state fluorescence anisotropy was measured using the same fluorimeter. The steady state fluorescence anisotropy, r, is defined by

$$r = \frac{(I_{VV} - G \cdot I_{VH})}{I_{VV} + 2G \cdot I_{VH}} \quad (1)$$

Here, I_{VV} and I_{VH} are the emission intensities obtained with the excitation polarizer oriented vertically and emission polarizer oriented vertically and horizontally, respectively. The G factor is the ratio of sensitivities of detection systems for vertically and horizontally polarized light $G = I_{HV}/I_{HH}$.

The fluorescence quantum yields were estimated from the corrected fluorescence spectra using Rhodamine 6G dye in ethanol ($\Phi_f = 0.94$ at 293 K) as secondary standard [32].

For the fluorescence quenching phenomenon, the fluorescence spectra were measured ($\lambda_{ex} = 295$ nm) at four different temperatures (293 K, 298 K, 303 K and 308 K). To confirm the quenching mechanism, the fluorescence quenching data were analyzed according to the following Stern–Volmer equation [33].

$$\frac{I_0}{I} = 1 + K_{SV}[Q] = 1 + k_q \tau_0 [Q] \quad (2)$$

where I_0 and I are the fluorescence intensities in absence and presence of the quencher, k_q and K_{SV} are the quenching rate constant and Stern–Volmer constant of the biological macromolecule, τ_0 is the fluorescence lifetime in absence of quencher and [Q] is the concentration of the quencher. For a static quenching phenomenon, the data were handled according to the modified Stern–Volmer equation [34].

$$\frac{I_0}{I_0 - I} = \frac{1}{f_a K_a} \cdot \frac{1}{[Q]} + \frac{1}{f_a} \quad (3)$$

In the present case, $(I_0 - I)$ is the difference in fluorescence in the absence and presence of the quencher at concentration [Q], f_a is the fraction of accessible fluorescence and K_a is the effective quenching constant for the accessible fluorophore.

Binding parameters

For the static quenching interaction, considering similar and independent binding sites in the biomolecule, the equilibrium between free and bound molecules is given by the following equation:

$$\log\frac{I_0 - I}{I} = \log K_b + n\log[Q] \tag{4}$$

where I_0 and I are the fluorescence intensities of BSA in absence and presence of PI, K_b and n are the apparent binding constant and number of binding sites, respectively.

Thermodynamic parameters

The acting forces for binding between the ligand and biomolecules include hydrogen bond, van der Wall force, electrostatic and hydrophobic interaction force and so on. To determine the nature of interaction between BSA and PI, thermodynamic parameters were calculated using the van't Hoff equation and the corresponding thermodynamic functions are based on the temperature effect.

$$\ln K_b = -\frac{\Delta H}{RT} + \frac{\Delta S}{R} \tag{5}$$

$$\Delta G = \Delta H - T\Delta S = -RT\ln K_b \tag{6}$$

ΔH, ΔS, and ΔG are enthalpy change, entropy change and free energy change, respectively, K_b is the binding constant at the corresponding temperature, T and R is the universal gas constant.

Fluorescence resonance energy transfer calculation

The energy transfer efficiency (E) is related not only to the distance (r) between the acceptor and the donor but also to the critical energy transfer distance or Förster radius (R_0) that is

$$E = \frac{R_0^6}{R_0^6 + r^6} = 1 - \frac{I}{I_0} \tag{7}$$

where I and I_0 are the fluorescence intensities of the donor in presence and absence of the probe, respectively. R_0 is calculated as

$$R_0 = 9.78 \times 10^3 [\kappa^2 \cdot n^{-4} \cdot \Phi_D \cdot J(\lambda)]^{1/6} \tag{8}$$

where Φ_D is the fluorescence quantum yield of the donor in the absence of the acceptor, κ^2 is the dipole orientation factor involving the geometry of the donor–acceptor dipoles, n is the refractive index of the medium. The spectral overlap integral, J, has been calculated as follows,

$$J = \frac{\int_0^\infty I_D(\lambda)\cdot\varepsilon_A(\lambda)\cdot\lambda^4\cdot d\lambda}{\int_0^\infty I_D(\lambda)\cdot d\lambda} \tag{9}$$

where I_D is the normalized donor emission spectrum and ε_A is the acceptor molar extinction coefficient.

Fluorescence lifetime measurements

All the fluorescence decays were obtained with a Time Correlated Single Photon Counting (TCSPC) set up employing a nanosecond diode laser (IBH, nanoLED-07) operating at λ_{ex} = 290 nm as the light source and TBX-04 as the detector. Instrument response function is ~90 ps. The fluorescence decay was collected with an emission polarizer kept at the magic angle (~54.7°). The decays were analyzed using Data Station v-2.5 decay analysis software. The fluorescence decay curves were analyzed by tri-exponential fitting program of IBH in order to obtain best residuals and acceptable χ^2 values. Intensity decay curves were obtained as a sum of exponential terms

$$F(t) = \sum_i a_i \exp\left(\frac{-t}{\tau_i}\right) \tag{10}$$

where $F(t)$ is the fluorescence intensity at time t, a_i the pre-exponential factor representing the fractional contribution to the time resolved decay of the ith component with a lifetime τ_i. Average lifetimes (τ_{avg}) of fluorescence were calculated from the decay times and pre-exponential factors using the following equation:

$$\tau_{avg} = \sum_i a_i \tau_i \tag{11}$$

CD measurements

The alteration in the secondary and tertiary structure of the protein in the presence of the probe was studied by monitoring circular dichroism (CD) on Jasco Corporation, J-815 CD spectrophotometer using a rectangular quartz cuvette of path length 1.0 mm at 1 nm data pitch intervals. All CD spectra were taken in a wavelength range 200–350 nm. The spectrophotometer was sufficiently purged with 99.9% nitrogen before starting the instruments. The spectra were collected at a scan speed of 100 nm/min and a response time of 1 s. Each spectrum was baseline corrected and the final plot was taken as an average of three accumulated plots. The α-helix content of BSA can be estimated according to the following equation:

$$\%\alpha - HelixContent = \frac{\theta_{MRD} - 2340}{30300} * 100 \tag{12}$$

where θ_{MRD} is the mean residue ellipcity at 222 nm in deg cm^2 - $dmol^{-1}$. It can be calculated as follows:

$$\theta_{MRD} = \frac{\theta_D(m\,deg)}{10 C_P L N_r} \tag{13}$$

where θ_D is the observed CD (mdeg) obtained in experiment, C_P is the BSA concentration (mol L^{-1}), L is the sample cell path length and N_r is the number of amino acid residues.

FT-IR measurements

FT-IR measurements were carried out at room temperature using Perkin–Elmer Spectrum-100 spectrophotometer. FT-IR spectra of free BSA and difference spectra [(BSA solution + PI solution) -/(PI solution)] in buffer solution were measured with 32 scans.

Molecular docking

The molecular docking was performed for getting the protein ligand binding energy and to identify the binding sites. For docking studies, we have used the PDB structure of BSA (PDB ID 3V03) (http://www.rcsb.org) [35]. The PDB structure of the probe was generated by the optimization of the structure with Gaussian 03 software [36] using Hartree–Fock method and 3-21G basis set. The docking experiments were achieved using the docking software AutoDock 4.2 [37] and AutoDock Tools (ADT). AutoDock generated different ligand conformers using a Lamarkian genetic algorithm (LGA), a GA implemented with an adaptive local method search. The energy based Autodock scoring function includes terms accounting for short range van der Waals and electrostatic interactions, loss of entropy upon ligand binding, hydrogen binding and solvation. For the recognization of the binding sites in BSA, docking was carried out and the grid size is set to 126, 98, 126 along x, y, z axes with a grid spacing of 0.453 Å after assigning the protein and probe with Kollman charges. The grid centre was set as −0.056, 0.011, −0.004 Å. At first AutoGrid was run to generate the grid map of various atoms of the ligand and receptor. After the

completion of grid map, AutoDock was run by using autodock parameters as, GA population size: 600 and maximum numbers of energy evaluations: 2.5×10^7 with numbers of generations 27,000. The total 100 numbers of run [38] were carried out; among these the minimum energy conformer was taken according to the ranking and scoring. In the docking run the root mean square tolerance was set to 2.0 Å.

Results and discussion

Spectral features of PI in solvents

Detail spectroscopic properties of PI in different solvents have already been studied by our group [4]. In water, PI shows large hypsochromic shifted absorption band at ~495 nm because of 'blue shift anomaly' observed generally in amino substituted molecules when dissolve in protic solvents [39,40]. Fluorescence intensity as well as fluorescence quantum yield in water is low compared to in acetonitrile (ACN) solvent due to greater hydrogen bond acceptor (HBA) ability of water (0.47) than acetonitrile (0.31). Similarly, fluorescence decay time of PI in water is reduced to 0.879 ns where that in ACN is 4.464 ns because of high non-radiative decay rate constants ($k^{nr} = 1.13 \times 10^9\ s^{-1}$ and $0.21 \times 10^9\ s^{-1}$ in H_2O and ACN, respectively). Our interest is to investigate the incorporation of this cationic dye PI inside the microheterogeneous environment of serum albumin.

Binding phenomenon of PI with protein

To explore the interaction between PI with BSA, we have measured absorption and emission spectra of PI in presence of BSA. The absorption and emission spectra of PI with increasing the concentration of BSA have been illustrated in Figs. 1 and 2a, respectively. Gradual addition of BSA in a buffer solution of PI results in steady red shift of the absorption maxima from ~495 nm to ~506 nm with concurrent enhancement of absorbance which reveals strong interaction between the two concerned partners. Enhanced solvation of the probe in hydrophobic protein cavity may be the reason of absorbance increment. Meanwhile, bathochromism of the absorption band of the protein bound dye PI can be explained in terms of decrease of local polarity around PI in the proteinous environment compared to pure buffer solution as the energy gap between the highest occupied molecular orbital (HOMO) and the lowest unoccupied molecular orbital (LUMO) of the dyes (Scheme S1) reduces to give rise to the observed red shift (Inset of Fig. 1). Our interpretation is further authenticated by a relative red shift of absorption maxima of PI on going from aqueous

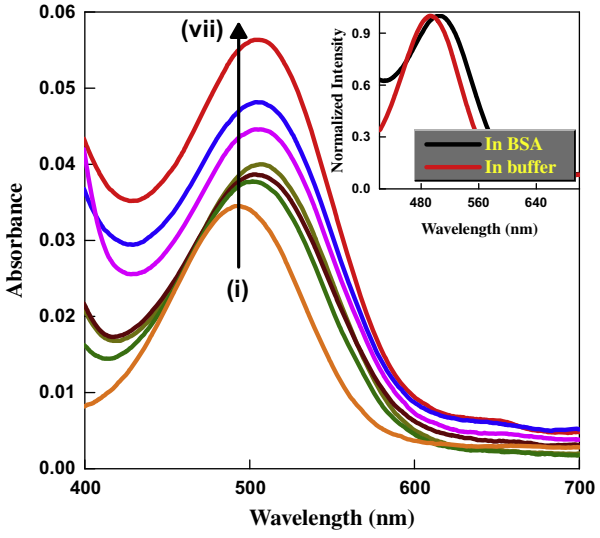

Fig. 1. Room temperature UV–vis absorption spectra of PI with increasing concentration of BSA (curves (i) → (vii) correspond to [BSA] = 0, 0.02, 0.03, 0.05, 0.06, 0.15 and 0.20 mM).

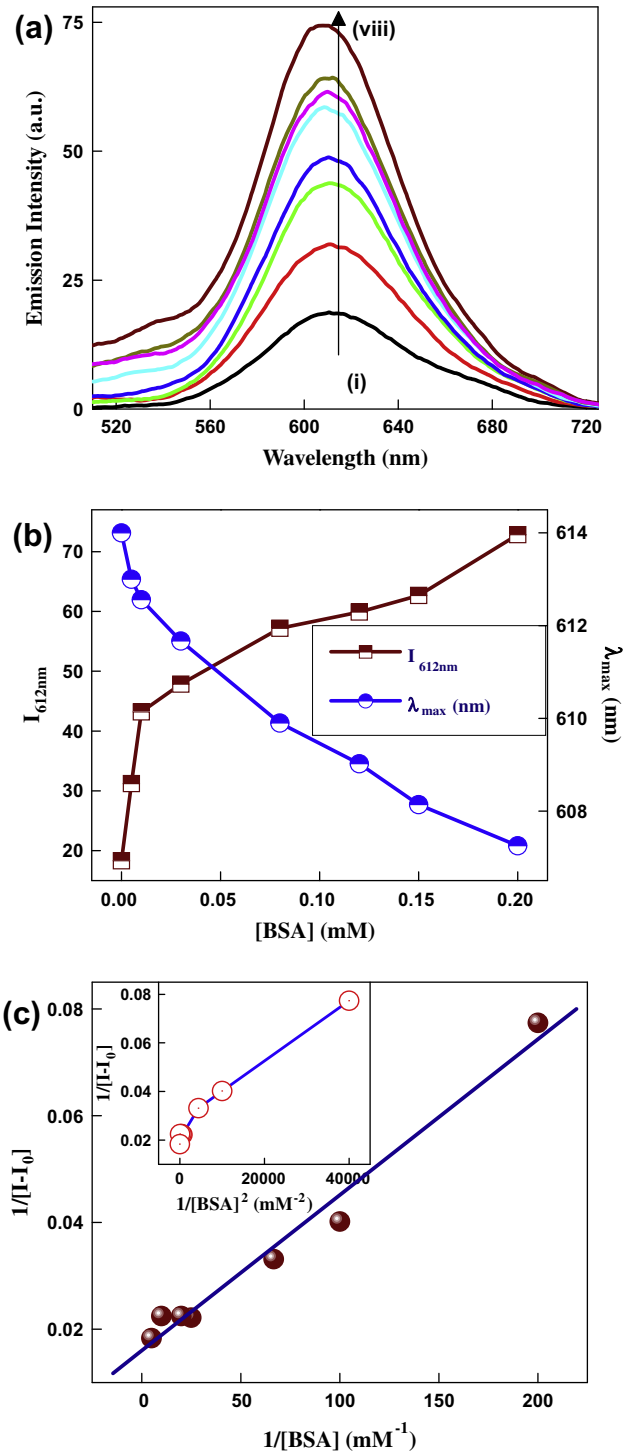

Fig. 2. (a) Room temperature fluorescence emission spectra (λ_{ext} = 495 nm) of PI with increasing concentration of BSA (curves (i) → (viii) correspond to [BSA] = 0, 0.005, 0.01, 0.03, 0.08, 0.12, 0.15 and 0.20 mM). (b) Variation of fluorescence intensity (I_{612nm}) and emission maxima (λ_{max}) of PI with increasing concentration of BSA. (c) Benesi–Hildebrand plot ($1/(I - I_0)$ vs $1/[BSA]$) for binding of PI with BSA (inset: plot of $1/(I - I_0)$ vs $1/[BSA]^2$ for 1:2 binding).

solution to a nonpolar medium like 1,4-dioxane (λ_{max} = 495 nm in water and λ_{max} = 535 nm in DOX), as discussed in our previous published article [4]. Fig. 2a exhibits manifold enhancement of fluorescence intensity of PI with slight blue shifting of the emission maximum from ~615 nm in buffer to ~607 nm in ~200 μM BSA. The corresponding enhancement of emission intensity as well as the extent of blue shifting has been picturized in Fig. 2b. It is known from our previous observation that water acts as a quencher of PI emission due to its high HBA basicity [4]. So encapsulation of the probe inside the hydrophobic cavity of protein shields it from outer aqueous environments, thereby enhances its emission intensity. On the other hand, blue shifting as observed with increasing BSA concentration (Fig. 2b) should not be mystified with observed red shift in the absorption profile (Fig. 1) as ground state and excited state behavior are completely different from each other [33]. The observed blue shift reflects the increase of hydrophobicity around the fluorophore. It is already reported [4] that the fluorescence quantum yield of PI in water is low compared to that in somewhat less polar medium. Hence, the increase in intensity and fluorescence quantum yield value (Table 1) on addition of protein may also support the existence of the probe inside the hydrophobic cavity of albumin. The non-radiative channels assisted by intermolecular hydrogen bonding present in aqueous solution are blocked to a great extent being less effective as the probe binds more and more with protein resulting in enhancement of fluorescence intensity and quantum yield values (Table 1). The strength of binding phenomenon occurring between BSA and PI may be estimated by the use of well known Benesi–Hildebrand relation. The complexation reaction with 1:1 stochiometry can be expressed as follows

$$\mathrm{PI} + \mathrm{BSA} \overset{K}{\leftrightarrow} \mathrm{PI:BSA}$$

$$K = \frac{[\mathrm{PI:BSA}]}{[\mathrm{PI}][\mathrm{BSA}]} \tag{14}$$

where K is the binding constant for the complexation equilibrium. The concentration terms for each component in Eq. (14) can be expressed in terms of fluorescence intensity. Assuming that the concentration of the probe–protein complex is very low compared to that of the free protein, the Benesi–Hildebrand relation for these types of complexation process can be written as follows,

$$I = \frac{I_0 + I_1 K[\mathrm{BSA}]}{1 + K[\mathrm{BSA}]}$$

Rearranging the above equation we have,

$$\frac{1}{(I - I_0)} = \frac{1}{(I_1 - I_0)} + \frac{1}{(I_1 - I_0)K[\mathrm{BSA}]} \tag{15}$$

where I_0, I and I_1 are the emission intensities in absence of, at intermediate and infinite concentration of BSA, respectively. The plot of $1/(I - I_0)$ vs $1/[\mathrm{BSA}]$ as depicted in Fig. 2c shows linear variation justifying 1:1 complexation between the fluorophore and protein with very high binding constant ($K = (5.47 \pm 0.89) \times 10^4\ \mathrm{M}^{-1}$). The non-linear plot of $1/(I - I_0)$ vs $1/[\mathrm{BSA}]^2$, as shown in inset of Fig. 2c, discards the probability of 1:2 binding case. The high binding constant value dictates strong binding ability of PI with BSA. From the determined K value, the free energy change ($\Delta G = -RT\ln K$) for the probe–protein binding process has been estimated to be −27.03 kJ/mol which indicates spontaneous complexation process.

Steady state fluorescence anisotropy

Complex biological membranes such as protein, DNA form highly organized molecular assemblies with considerable degree of rigidity. Steady-state fluorescence anisotropy (r) studies are of immense importance in the field of biochemical applications as they provide valuable information regarding the precise location of the probe in complex molecular assembly. Any modulation in the rigidity of the surrounding environment of the fluorophore, like shape, size, and flexibility affects the observed anisotropy. The so-called environment induced motional restriction on the mobility of the probe in biological membranes is manifested through anisotropy variation and thereby furnishing clues to assess the probable location of the probe in the microheterogeneous bio-environments like proteins, DNA, and micelles [26–29]. Fig. 3 depicts the anisotropy variation of PI with increasing the concentration of BSA. Addition of BSA to the solution of PI leads to enhancement of anisotropy value upto 80 μM and then attains constancy. The maximum value of anisotropy faced by PI is 0.265 for 200 μM of BSA pointing towards the fact that considerable restriction is imposed on the mobility of the probe inside the microheterogeneous medium with increasing protein concentration. This high value of r also dictates stronger binding ability of PI with BSA thereby complimenting the value of K and ΔG.

Time resolved fluorescence of PI in presence of protein

Fluorescence decay analysis of PI (fixed concentration) in the absence and presence of BSA has been illustrated in Fig. S1 and Table 1, respectively. The data have been best fitted by bi- and tri-exponential way to get better residuals and acceptable χ^2 values. With increasing BSA concentration, the fluorescence decay time of probe increases. As the probe becomes much more encapsulated within the hydrophobic pocket of BSA and exposure of the probe to water is less, the non-radiative decay channels operating in aqueous medium are reduced. The non-radiative decay rate constants (k^{nr}) can be calculated using the following equation:

$$k^{nr} = \frac{1 - \Phi_F}{\tau_{avg}} \tag{16}$$

Increase of fluorescence quantum yield (Φ_F) value with increasing protein concentration listed in Table 1 indicates less operative non-radiative decay channels which are further justified by k^{nr} values. From Table 1, it can be easily concluded that with increasing BSA concentration, non-radiative decay channels become less operative thereby enhancing its decay time, fluorescence intensity as well as quantum yield values.

Influence of PI concentration on the BSA fluorescence intensity

Room temperature emission and absorption spectra of BSA with addition of probe, PI, are portrayed in Fig. 4a and b, respectively. It

Table 1
Fluorescence decay parameters of PI in aqueous buffer and proteinous media.

Medium	τ_1 (ns)	τ_2 (ns)	τ_3 (ns)	τ_{avg} (ns)	χ^2	Φ_F ($\times 10^{-2}$)	κ^{nr} ($\times 10^{10}\ s^{-1}$)
Buffer	0.84 (0.94)	1.56 (0.06)	–	0.88	1.17	1.77	1.118
10 μM BSA	1.44 (0.86)	7.30 (0.14)	–	2.26	1.21	3.65	0.426
80 μM BSA	3.54 (0.37)	9.90 (0.10)	0.85 (0.53)	2.75	1.14	4.79	0.346
200 μM BSA	3.80 (0.38)	10.22 (0.10)	1.02 (0.52)	3.00	1.11	4.95	0.316

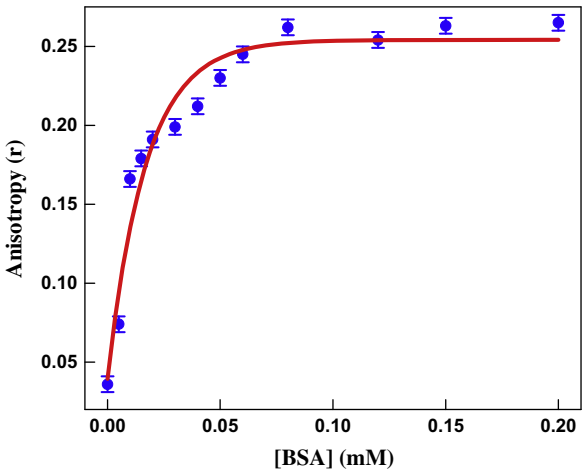

Fig. 3. Variation of steady state fluorescence anisotropy (r) of the chromophore PI with increasing concentration of bovine serum albumin.

is seen that the intrinsic fluorescence intensity of BSA decreases gradually with increasing PI concentration (Fig. 4a). BSA has two tryptophan residues, Trp-213 and Trp-134. Since Trp-213 and Trp-134 are located at hydrophobic subdomain IIA and hydrophilic subdomain IB, respectively, the emission spectra of Fig. 4a is originated mainly from Trp-213. As emission spectrum of PI has very low intensity on 295 nm excitation, addition of probe has too small contribution on the fluorescence intensity of BSA. In order to establish whether the quenching of BSA is static or dynamic in nature, we have carried out temperature dependence experiment. The Stern–Volmer plot according to Eq. (2) for the quenching of BSA by PI at four different temperatures 293 K, 298 K, 303 K, and 308 K are displayed in Fig. 4c. Since the plots are linear and increasing temperature does not change the linearity of the Stern–Volmer plot indicating the occurrence of a single type of quenching phenomenon, either static or dynamic. In case of dynamic quenching, with increase of temperature faster diffusion occurs thereby showing larger amount of dynamic quenching. But in the case of static quenching, due to dissociation of the ground state complex, smaller amounts of quenching may occur. From Table 2, the values of K_{SV} and k_q are found to be decrease with increasing temperature and k_q is greater than the value of the maximum scatter collision quenching constant ($2 \times 10^{10}\ M^{-1}\ s^{-1}$) [41]. One additional method to make a distinction between static and dynamic quenching is by observing the changes of the absorption spectra of the fluorophore in the absence and in presence of the fluorophore. Since dynamic quenching is excited state phenomenon of the fluorophore, no changes in the absorption spectra is expected. Conversely, ground-state complex formation will perturb the absorption spectra of the fluorophore thereby implying static quenching phenomenon. Fig. 4b dictates that differences in the absorption spectra of BSA occur in presence of the probe. These results conclude that the probable fluorescence quenching mechanism of BSA by PI is static in nature.

The mechanism of fluorescence quenching of BSA by the studied probe is further analyzed by time resolved measurements. Static quenching i.e. ground state complex formation, does not diminish the decay time of the fluorophore because the uncomplexed chromophores have the unquenched lifetime (τ_0). Typical decay profiles of BSA (fixed concentration) in presence of different amounts of probe are displayed in Fig. S2 with their residual fit and their relative data are tabulated in Table 3. Since BSA exhibits multi-exponential decays due to the existence of the conformational isomers of tryptophan, we have not attempted to the individual contribution. Rather the average lifetime values calculated using

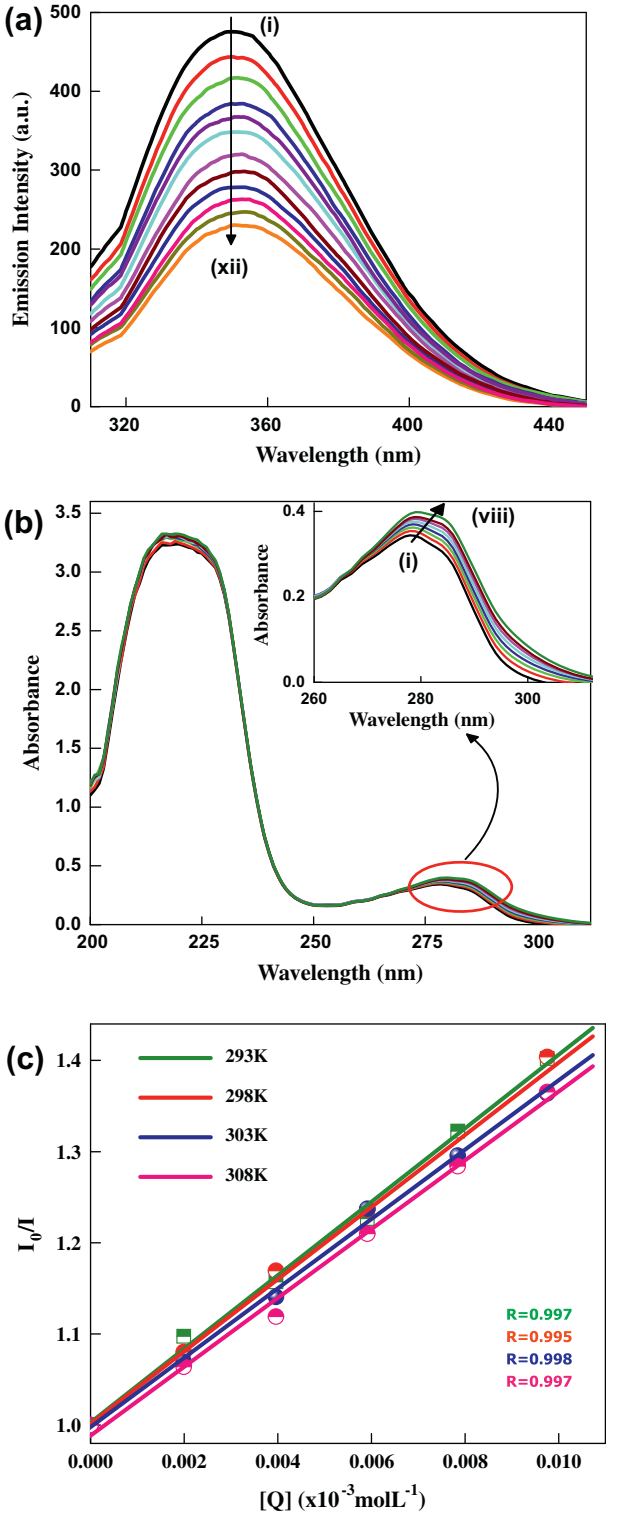

Fig. 4. Effect of increasing concentration of PI on the (a) fluorescence spectra on 295 nm excitation (curves (i) → (xii) correspond to [PI] = 0, 2, 4, 6, 8, 10, 12, 14, 15, 17, 19, 21 μM) and (b) absorption spectra of BSA (10 μM) at 293 K ((i) → (viii) corresponds to 0, 2, 4, 6, 8, 10, 15, 20 μM of PI concentration). (c) Stern–Volmer plots for the interaction of PI with BSA at 293 K, 298 K, 303 K and 308 K.

Eq. (11) has been utilized for quantitative analysis. The reduction in decay times in different probe: protein ratios are very marginal (5.01–4.90 ns) recommending the formation of ground state complex between the probe and BSA. This result reconfirms that the quenching of Trp-213 fluorescence by probe is static in nature.

Table 2
Quenching and thermodynamic parameters for the interaction of PI with BSA at different temperature.

Temperature (K)	K_{SV} ($\times 10^4$ M^{-1})	k_q ($\times 10^{12}$ M^{-1} s^{-1})	K_a ($\times 10^4$ M^{-1})	K_b ($\times 10^4$ M^{-1})	n	ΔG (kJ mol^{-1})
293	4.03 ± 0.14	4.03 ± 0.14	6.05 ± 0.19	6.00 ± 1.52	1.03	−26.80
298	3.96 ± 0.20	3.96 ± 0.20	3.63 ± 0.19	8.78 ± 1.45	1.06	−28.20
303	3.80 ± 0.11	3.80 ± 0.11	1.72 ± 0.14	28.20 ± 1.37	1.16	−31.61
308	3.77 ± 0.15	3.77 ± 0.15	1.23 ± 0.20	43.39 ± 1.53	1.20	−33.24

Table 3
Fluorescence lifetime of different BSA-ligand ratios.

BSA:PI	τ_1 (ns)	τ_2 (ns)	τ_3 (ns)	τ_{avg} (ns)	χ^2
1:0.0	4.17 (0.34)	1.12 (0.16)	6.82 (0.50)	5.01	1.09
1:0.25	0.93 (0.15)	4.43 (0.44)	7.11 (0.41)	5.00	0.99
1:0.6	3.21 (0.29)	0.53 (0.14)	6.59 (0.57)	4.76	1.04
1:1	3.74 (0.29)	1.15 (0.15)	6.66 (0.56)	4.99	1.18
1:1.4	4.38 (0.38)	1.13 (0.19)	6.99 (0.43)	4.88	1.06
1:2	1.04 (0.16)	4.13 (0.40)	7.00 (0.44)	4.90	0.99

Table 4
3D-fluorescence spectral characteristics of BSA and BSA–PI system.

System	Peak I ($\lambda_{ex}/\lambda_{em}$)	$\Delta\lambda$ (nm)	Intensity	Peak II ($\lambda_{ex}/\lambda_{em}$)	$\Delta\lambda$ (nm)	Intensity	Intensity ratio
BSA	280/354	74	848.12	235/354	119	276.57	3.07:1
BSA–PI	275/349	74	505.52	240/349	109	167.06	3.02:1

The fluorescence quenching of BSA by PI can also be analyzed by modified Stern–Volmer Eq. (3) as the quenching of BSA by PI originates from the formation of a complex. The corresponding plots are shown in Fig. 5a and the values of K_a at different temperatures are listed in Table 2. The decreasing trend of K_a with increasing temperature is in accordance with K_{SV}'s dependence on temperature which reconfirms the static quenching phenomenon.

Association constants and number of binding sites

For the static quenching interaction, if it is assumed that there are similar and independent binding sites in the biomacromolecule, the binding constants (K_b) and number of binding sites (n) can be determined using Eq. (4). By the plot of $\log((I_0 - I)/I)$ vs $\log[Q]$ (Fig. 5b), the K_b as well as n per BSA can be evaluated and are enlisted in Table 2. The value of K_b (6.00×10^4 M^{-1}) is quite similar to that of K value (5.47×10^4 M^{-1}) obtained from Benesi–Hildebrand plot (Fig. 2c). The approximate value of n is equal to 1 at different temperature indicating the existence of just a single binding site in BSA for PI. In BSA, the tryptophan residues involved in binding could be either Trp-134 or Trp-213. Of both tryptophans in BSA, Trp-134 is more exposed to a hydrophilic environment, whereas Trp-213 is deeply buried in the hydrophobic loop [25]. So, from the value of n, it is proposed that PI is more likely to bind to the hydrophobic pocket of BSA, i.e. to Trp-213 located in subdomain IIA.

Thermodynamic parameters and nature of the acting forces

Essentially, the interaction forces for binding between drugs and biomolecules include hydrogen bond, van der Wall force, electrostatic and hydrophobic interaction force and so on. Since the signs and magnitudes of the thermodynamic parameters (ΔH, ΔS, ΔG) can account for the main driving forces for this probe–protein interaction, these parameters were estimated from the plot of ln K_b vs $1/T$ (Fig. 5c) according to the vant Hoff Eq. (5) and thermodynamic Eq. (6) (Table 2). Ross and Subramanian [42] summed up the thermodynamic law to evaluate the primary mode of binding force between drugs and biological molecules: (1) $\Delta H > 0$ and $\Delta S > 0$ are associated with hydrophobic interaction; (2) electrostatic force are more dominant when $\Delta H \cong 0$ and $\Delta S > 0$; (3) $\Delta H < 0$ and $\Delta S < 0$ are frequently taken for hydrogen bond and van der Waals force. In the present case, the positive value of ΔH (106.49 kJ mol^{-1}) and ΔS (0.45 kJ mol^{-1} K^{-1}) indicate that hydrophobic interaction plays the major role during probe–protein binding process. From Table 2, the negative values of ΔG signify that the process of drug–protein interaction is spontaneous in nature.

Energy transfer efficiency

Fluorescence resonance energy transfer (FRET) is a non-destructive spectroscopic method that monitors the close proximity and relative angular orientation of the chromophores. According to Förster's non-radiative energy transfer theory, the efficiency of FRET depends on the relative orientation of the donor and acceptor dipoles, the extent of overlap between the donor emission and the acceptor absorption and the distance between the donor and acceptor [43]. It has been already reported for BSA that $\kappa^2 = 2/3$, $n = 1.333$ and $\Phi_D = 0.15$ [28]. Overlap integral, J, has estimated by integrating the overlapping region of the UV absorption of probe and the emission spectra of protein (Fig. S3) using Eq. (9) which is 3.226×10^{-15} cm^3 L mol^{-1}. Using these values we can calculate $R_0 = 2.12$ nm, $E = 0.22$ and $r = 2.61$ nm. So the distance between PI and tryptophan residues of BSA is 2.61 nm (<8 nm) indicating high probability of energy transfer from protein to probe. This method of distance measurement for BSA may be confusing because of the presence of two tryptophan residues (Trp-213, Trp-134) in BSA. The distance estimated here is actually the average value between the probe and the tryptophan residues. The result of $r > R_0$ again confirms the presence of static quenching process between PI and BSA.

The effect of ions on the binding constant of probe–protein interaction

The presence of some metal ions like Ca^{2+}, Zn^{2+}, Ni^{2+}, Co^{2+}, Mg^{2+}, and Cu^{2+} in the blood plasma can influence the binding of the drug to serum albumin. To explore the effect of these metal ions on the binding of PI to BSA, the quenching constants of BSA–PI in presence of different cations have been determined and are as follows: for

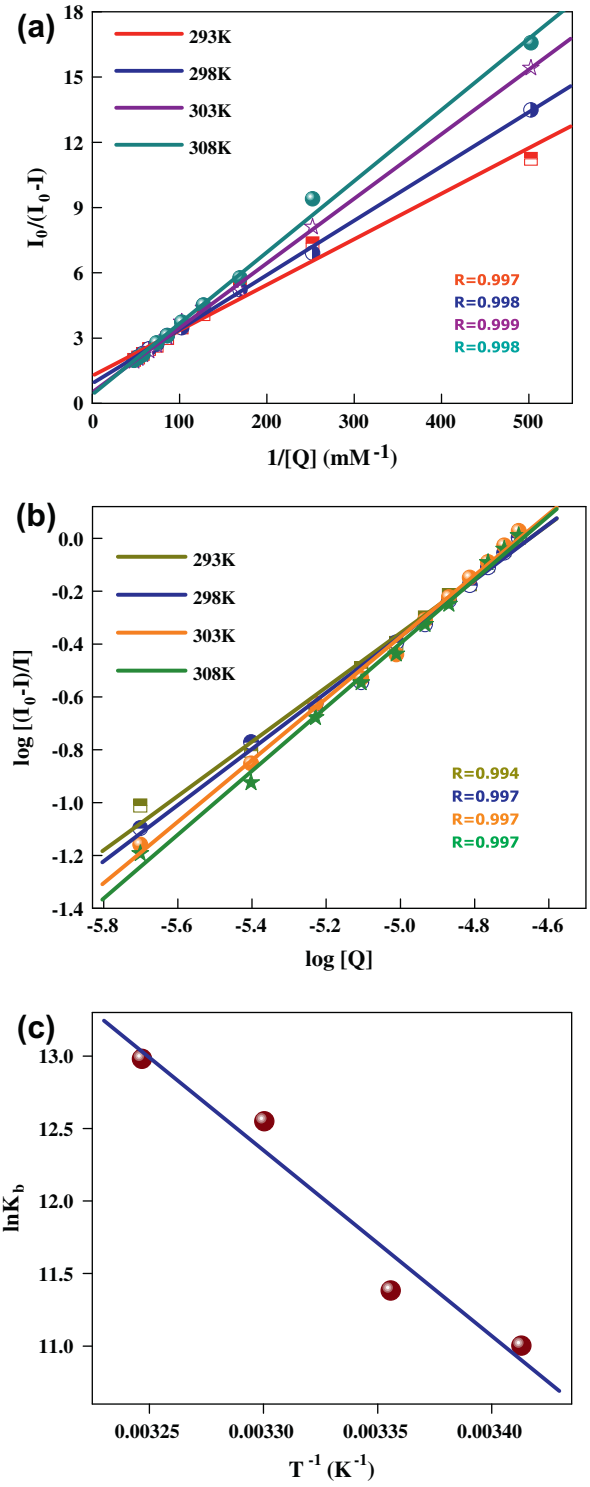

Fig. 5. (a) Modified Stern–Volmer plot for the binding phenomenon between PI and BSA at four different temperatures. (b) Plots of $\log((I_0 - I)/I)$ vs $\log[Q]$ to obtain number of binding sites of BSA for PI. (c) van't Hoff plot for the binding of PI with BSA.

Zn^{2+}, $K_a = 3.56 \times 10^4\ M^{-1}$; Ca^{2+}, $K_a = 3.05 \times 10^4\ M^{-1}$; Mg^{2+}, $K_a = 3.25 \times 10^4\ M^{-1}$ and Cu^{2+}, $K_a = 3.60 \times 10^4\ M^{-1}$. The constants of drug–protein interaction decrease by 41–50% in presence of these bivalent metal ions. This reduction in K_a values indicates that the drug as well as the metal ions competes for the same binding site in BSA at the same time. The formation of metal ion–albumin complexes is likely to affect the conformation of protein, which may influence PI binding kinetics and even inhibit PI–BSA binding. Therefore, these metal ions shorten the storage of the probe in the protein cavity and increase the contents of free drug.

Identification of binding location of PI on BSA

We already know that BSA consists of three homologous domains called I–III and each domain contains two subdomains (A and B). The principle regions of probe–protein interaction are subdomain IIA and IIIA which are characterized as Sudlow's site I and II, respectively. To identify the precise location of binding of the probe inside the hydrophobic zone of the protein, we have executed the site specific binding experiment using phenylbutazone (PB) for Sudlow site I and flufenamic acid (FF) for site II (Fig. S4). The probe PI has been injected simultaneously into a system in which the concentration of BSA and site marker is 1:1. The probe has to interact with the site markers to get the chance to bind with BSA if they bind to BSA in the same site. The binding constant for the interaction phenomenon between PI and BSA should be decreased in presence of site markers if binding occurs in the same place. Binding constant obtained using Eq. (4) are as follows: $K_b = 1.38 \times 10^4\ M^{-1}$ and $2.40 \times 10^4\ M^{-1}$ for PI–BSA system in presence of PB and FF, respectively. The binding constant in presence of PB is much smaller than that for the absence ($6.0 \times 10^4\ M^{-1}$) as well as with the presence of FF. These reveal that PI mainly competes with PB in subdomain IIA indicating that the probe binds to BSA in Sudlow site I.

Identification of conformational changes on BSA by PI

Synchronous fluorescence spectroscopy studies

The synchronous fluorescence spectroscopy launched by Lloyd [44] is a powerful tool for exploring the conformational changes of protein by external probe. This method involves simultaneous scanning of excitation and emission monochromators of a fluorimeter while maintaining a fixed wavelength difference ($\Delta\lambda$) between them. When $\Delta\lambda$ is set at 15 nm and 60 nm, synchronous fluorescence spectra offer the characteristics of tyrosine and tryptophan residues of BSA. Any shift in the emission maximum indicates a change in the polarity of the surrounding environment of tyrosine and tryptophan residues of BSA. Synchronous fluorescence spectra of tyrosine and tryptophan residues of BSA at various concentration of PI are shown in Fig. S5. Comparing Fig. S5a and b we can easily conclude that the fluorescence of BSA is mainly originated from that of tryptophan residues. The emission peaks shown in Fig. S5a do not shift over the investigated concentration range which signifies little effect on the microenvironment of tyrosine residue of BSA by probe. On the other hand, when $\Delta\lambda = 60$ nm, the maximum emission wavelength undergoes a blue shift of 4 nm from 282 nm to 278 nm (Fig. S5b). The blue shift of the emission maximum indicates that the conformation of BSA is altered and the polarity around the tryptophan residues is decreased and the hydrophobicity is increased in presence of PI.

3D-fluorescence spectroscopy

To get additional information or evidence regarding the conformational changes of BSA in presence of PI, 3D-fluorescence spectroscopy has been employed. The conformational changes of this serum albumin have been obtained by comparing the spectral modification in absence and in presence of the studied probe. Fig. S6 displays the corresponding map of BSA and BSA–PI systems and the relevant data are enlisted in Table 4. Two typical fluorescence peaks (peak I and peak II) could be easily found in the 3D-fluorescence spectra of BSA and BSA–PI systems. These are the lower right of the first-ordered Rayleigh scattering peak (A, $\lambda_{ex} = \lambda_{em}$) and the left of the second ordered Rayleigh scattering peak (B, $\lambda_{em} = 2\lambda_{ex}$). Peak I ($\lambda_{ex} = 280$ nm and $\lambda_{em} = 354$ nm) mainly

reveal the spectral behavior of tryptophan and tyrosine residues. From the UV–vis absorption spectra of BSA (Fig. 4b) it is seen that there is an absorption peak at ~277 nm arising by the $\pi \rightarrow \pi^*$ transition of aromatic amino acid in BSA as the tryptophan, tyrosine and phenylalanine in the binding cavity of protein have conjugated π electrons thereby forming charge transfer complex with other electron or π-electronic system. Besides peak I, there is another strong fluorescence peak II (λ_{ex} = 235 nm and λ_{em} = 354 nm) and BSA has strong absorption peak at 212 nm (Fig. 4b). Considering these two phenomenon, it can be inferred that peak II is mainly originated by $n \rightarrow \pi^*$ transition of BSA with characteristics polypeptide backbone structure. The quenching of the fluorescence intensity of the two peaks of BSA (40% for peak I and 39% for peak II) and the blue shifting of the maximum emission wavelength after addition of PI (Table 4) suggest a less polar environment of both residues. This result is consistent with the results of synchronous fluorescence spectra (Fig. S5). Thus we may conclude that addition of PI changes the polarity of the microenvironment result in conformational changes of BSA.

Circular dichroism and FT-IR study

To monitor the change of secondary structure of albumin upon interaction with ligand, circular dichroism (CD) experiment has been carried out and the results are shown in Fig. 6. In the CD spectrum BSA exhibits two negative bands at 208 nm and 222 nm in the ultraviolet region which are contributed from $n \rightarrow \pi^*$ transition of the peptides inter linkage of α-helix [45]. With increasing the addition of PI, the band intensity increases regularly without any significant shift of the peaks. The quantitative analysis of the α-helix content can be estimated using Eq. (12) and are shown in Fig. 6. The % of α-helix content is found to be increased from 58.12% in pure BSA to 62.17% in presence of PI signifying that binding of PI to BSA induces some conformational changes. The increase of α-helix content points towards the fact that PI combines with the amino acid residues of the main polypeptide chain of protein and perturbs interior electrostatic networks. Increase in θ_{MRD} points toward the stabilization of protein upon binding with ligand. So these phenomena in accordance with synchronous and 3D-fluorescence spectroscopy establish that PI interacts with BSA by causing slight unfolding of the polypeptide of protein and conformational changes. Actually, the binding of PI to BSA changes the secondary structure of protein, especially α-helix structure.

Since infrared spectroscopy has long been used as a powerful tool for investigating the secondary structure of protein, FT-IR method has been applied here to gain a better understanding of this probe–protein binding interaction. Particularly, the amide I band is more useful than amide II band for the study of secondary structure and it originates at 1600–1700 cm^{-1} (mainly C=O stretch) [46]. Since we are interested to test the changes of amide I bands, FT-IR spectra of free BSA and PI-bound BSA have been measured in the wavelength range of 1600–1700 cm^{-1}. It is seen that the peak positions of amide I band (1634 cm^{-1}, broad spectrum) has no shift (figure not shown) after addition of PI, but its intensity remarkably decreases from that of free BSA. Changes of the protein secondary structure may be the reason of the decrease in the intensity of amide I band.

Structural stability of protein by probe binding

Binding of probe to a protein may stabilize or destabilize its structure. In order to investigate structural stability of BSA in presence of PI, we have executed chaotrope induced unfolding of protein by monitoring the tryptophan fluorescence through exciting at 295 nm. Denaturation does not affect the primary structure of protein but it disrupts both the secondary and tertiary structure of proteins, i.e. total or partial loss of three dimensional structures. Proteins can be denatured by heat, pH or chemical denaturants such as urea, a strong denaturing agent [27–29]. The plot of relative fluorescence intensity of protein (I_0 and I in absence and presence of chaotrope) and probe–protein complex with variation of urea concentration are found to be sigmoidal in nature (Fig. S7).

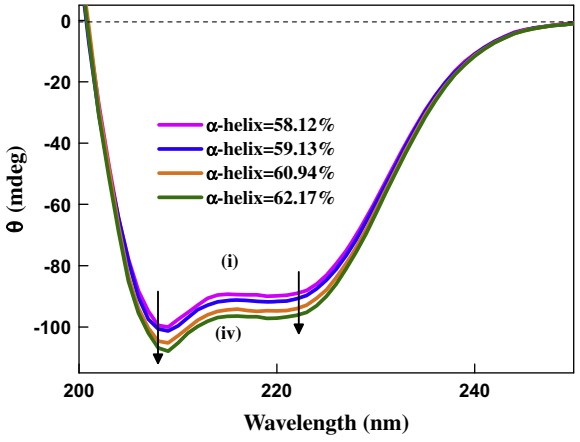

Fig. 6. Circular dichroism spectra of BSA with variation of concentration of PI ([BSA] = 10 μM and [PI] = 0, 10, 20, 40 μM for (i) to (iv)).

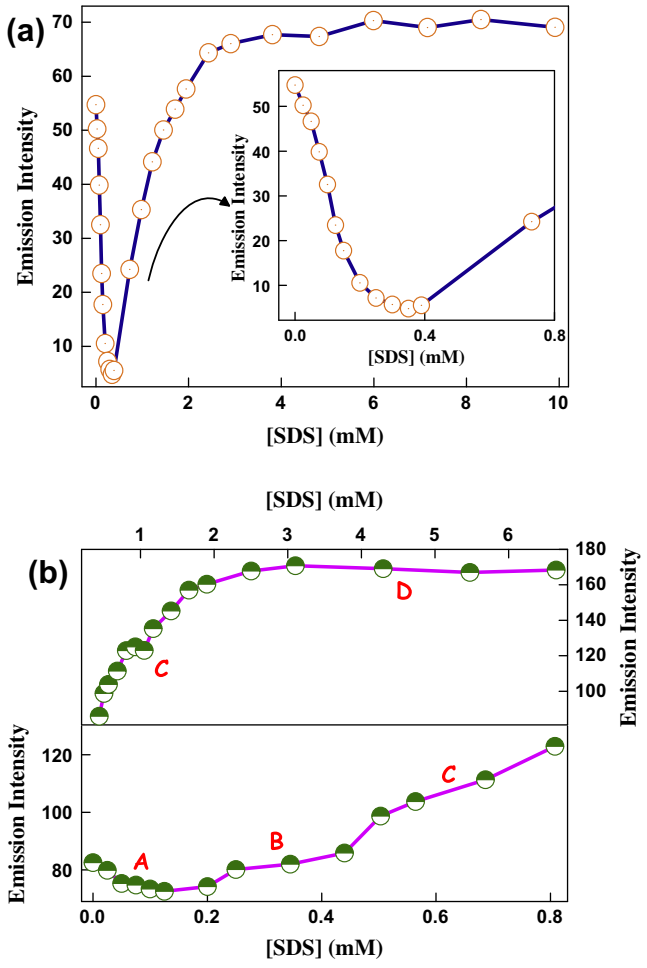

Fig. 7. (a) Fluorescence intensity (at emission peak) of PI (20 μM) in Tris buffer as a function of SDS concentration. Inset: magnified view of the changes in the emission profile of PI at low SDS concentration region. (b) Variation of emission intensity (at 614 nm) of PI (20 μM) bound to BSA (100 μM) with increasing concentration of SDS.

As shown in this figure, the intrinsic fluorescence of protein decreases with addition of urea from 0 to 8.5 M. The urea concentration for the half completion of denaturation of protein, i.e. $(den)_{1/2}$ is more for probe bound protein compared to that of bare protein thereby indicating the stabilization of the protein in the presence of the present dye, PI.

Competitive binding of surfactant with probe and protein

The effect of anionic surfactant SDS on the spectral properties of PI has been reported earlier [4]. Fig. 7a shows the changes in emission intensity at the peaks of the emission spectra of PI in Tris buffer upon addition of SDS. On addition of SDS far below CMC, the emission intensity decreases gradually to reach a minimum and then begins to grow up to reach the maximum. The decrease in fluorescence intensity (far below CMC of SDS) can be explained in terms of the formation of association complexes involving propidium cation and dodecyl sulfate anion. Further increase in SDS concentration increases the fluorescence intensity of PI indicating increase in solubilization of PI in micelle. At higher SDS concentration, all the dye molecules are compartmentalized into the micelle and protected from proton transfer mechanism due to shielding from bulk water. But different surveillance is occurred in presence of protein BSA. The binding isotherm of BSA with surfactant shows four characteristic regions (A, B, C, D) as already mentioned by

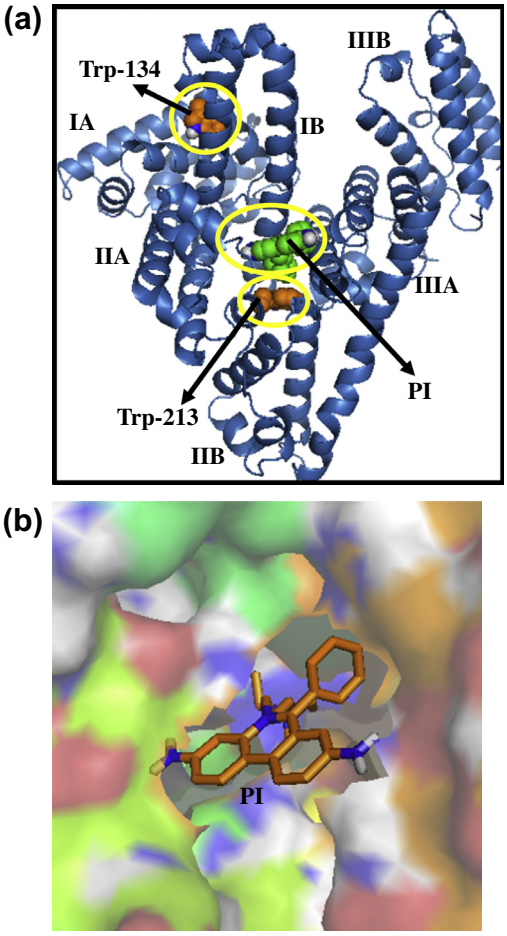

Fig. 8. (a) Cartoon picture of final conformation obtained after energy minimization followed by equilibration of the PI–BSA composite system. PI and two tryptophan residues (Trp-134 and Trp-213) are shown in space-filling model. (b) Cartoon picture of enlarged binding mode between PI and BSA. The ligand structure is shown using ball-and-stick model.

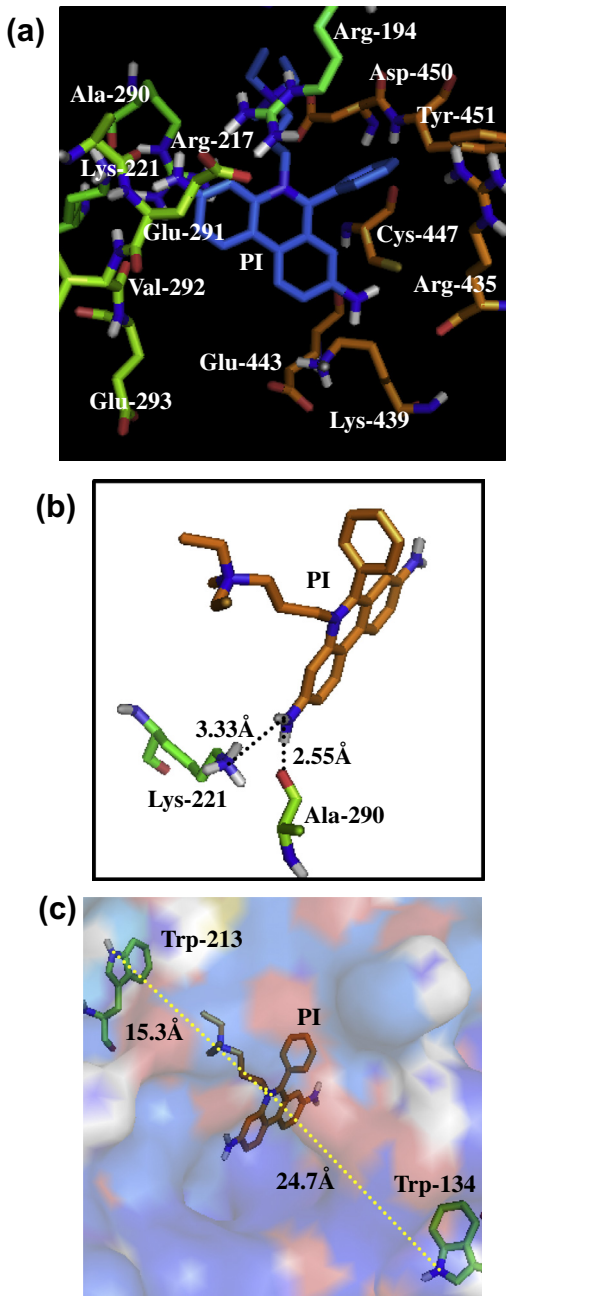

Fig. 9. (a) Docking pose of various residues of BSA, the residue present within <5 Å of the probe PI. (b) Detailed illustration of H-bond between PI and Lys-221, Ala-290, and (c) the distance between PI and tryptophan residues (Trp-134 and Trp-213). The residues of BSA and the ligand structure are represented using ball-and-stick model.

several groups [27–29]. But what will happen in presence of a cationic dye, whether the anionic surfactant binds with protein or with cationic dye? The plot of emission intensity of PI–BSA complex against SDS concentration is shown in Fig. 7b. As can be seen from the plots, here also the curve can be divided in to four distinct regions similar to binding isotherm of BSA in presence of SDS. Specific binding occurs in regions A up to 0.125 mM SDS concentration. The most important part of SDS–BSA interaction after region B is termed as the cooperative region where emission intensity sharply increases which is similar to that of the observation in case of protein-SDS binding curve. This indicates that massive binding of the surfactant begins to occur on the protein leading to its uncoiling process. Due to unfolding of BSA, the number of hydrophobic binding sites increases. So the emission intensity

increases as the probe molecule gets more and more solubilization in the hydrophobic region and senses increasing hydrophobicity of its surrounding environment. After region C, with increasing SDS concentration, there is no significant change in emission intensity as it reaches at saturation region D where further binding of the surfactant does not occur on the protein. Since emission profile (Fig. 7b) matches well with the BSA–SDS binding isotherm, binding interaction of SDS mainly occur with BSA. So PI can be endorsed to the competitive nature of binding between SDS and PI towards BSA.

Molecular docking analysis

Among the various conformers of docking results, the minimum energy conformer has been taken on the basis of free energy of binding and score ranking [47]. The minimum binding energy conformer is shown in Fig. 8. We have already stated that there are two drug binding sites, namely site I and site II located in the hydrophobic cavities in sub domain IIA and IIIA respectively [48]. The minimum energy conformer reveals that our ligand PI binds within sub domain IIA (Fig. 8a). The probe, PI, is surrounded by the hydrophobic side chains and also by the positively charge residue, namely, Ala-290, Val-292, Cys-447, Tyr-451 and Arg-194, Arg-217, Lys-221, Lys-439, Arg-435, etc. respectively as shown in Fig. 9a. Therefore, we can conclude that the interaction between PI and BSA is mainly hydrophobic in nature. Also there are a numbers of hydrogen bonding and electrostatic interactions, due to the presence of several ionic and polar groups (Glu-291, Glu-293, Glu-443) near the probe. Taking the distance between donor and acceptor atom 2.6–3.5 Å [38,47,49], we account two hydrogen bonds between amino group of PI and the adjacent O atom of Ala-290 (2.55Å) and N atom of Lys-221 (3.33 Å) in Fig. 9b. Also hydrogen bonding supports that the hydrophilicity decreases instead of increasing the hydrophobicity with in the BSA–PI complex [38,47]. The observed free energy change of binding (ΔG) for the BSA + PI complex obtained from the docking simulation is -4.35 kcal mol^{-1}, which is less comparable to our experimental free energy of binding (-6.43 kcal mol^{-1}) obtained from complexation study by Benesi–Hildebrand plots. This difference in experimental and theoretical results may be due to exclusion of the solvent in docking simulations or rigidity of the receptor other than tryptophan [38,49]. The distance between tryptophan and our target probe obtained from FRET calculation (2.61 ± 0.01 nm) is also comparable from the distance obtained from docking simulation where distances are 1.53 ± 0.02 nm and 2.47 ± 0.01 nm for Trp-213 and Trp-134 respectively (Fig. 9c). The docking study also supports that the increase in emission intensity of the probe PI is mainly due to the complexation and movement of the probe from the more polar hydrophilic region to the less polar hydrophobic region.

Conclusion

In this article, the interaction of PI, a well-recognized DNA intercalating dye, with the model protein BSA have been investigated using various spectroscopic methods including UV–vis, steady state and time resolved fluorescence measurements, anisotropy study and CD spectroscopy. The experimental data indicates that the quenching mechanism between BSA and PI is static in nature, i.e. ground state complex formation with very high binding constant ($\sim 10^4$ M^{-1}), this binding phenomenon is spontaneous and hydrophobic interaction plays a crucial role in this reaction. The synchronous and 3D-fluorescence spectroscopy as well as CD study and FT-IR measurements point towards the fact that secondary structure of the protein slightly changes in presence of PI. Site-competitive replacement experiment using phenylbutazone and flufenamic acid has validated the binding of probe to Sudlow site I of BSA. Molecular docking has been employed to further relocate the specific binding sites, the results of which are identical to the experimental findings. Chaotrope induced fluorescence studies of BSA and BSA–PI systems signifies enhanced stabilization of protein structure upon binding with the dye, PI. A competitive binding phenomenon is observed between BSA and PI towards SDS.

Acknowledgements

NG acknowledges DST, India (Project no. SR/S1/PC/26/2008) for financial support and AS thanks CSIR, New Delhi, for her research fellowship and SJ and DR thank UGC, for their research fellowship.

Appendix A. Supplementary material

Supplementary data associated with this article can be found, in the online version, at http://dx.doi.org/10.1016/j.saa.2013.10.049.

References

[1] T. Kral, K. Widerak, M. Langner, M. Hof, J. Fluoresc. 15 (2005) 179–183.
[2] L. Zamai, E. Falcieri, G. Marhefka, M. Vitale, Cytometry 23 (1996) 303–311.
[3] D.L. Garner, L.A. Johnson, Biol. Reprod. 53 (1995) 276–284.
[4] A. Samanta, B.K. Paul, N. Guchhait, J. Photochem. Photobiol. B 109 (2012) 58–67.
[5] A. Krishan, J. Cell Biol. 66 (1975) 188–193.
[6] H. Lecoeur, Exp. Cell Res. 277 (2002) 1–14.
[7] D.L. Garner, L.A. Johnson, S.T. Yue, B.L. Roth, R.P. Haugland, J. Androl. 16 (1994) 620–629.
[8] B. Ahmad, S. Parveen, R.H. Khan, Biomacromolecules 7 (2006) 1350–1356.
[9] S. Monti, I. Manet, F. Manoli, M.L. Capobianco, G. Marconi, J. Phys. Chem. B 112 (2008) 5742–5754.
[10] G. Zhang, B. Keita, C.T. Craescu, S. Miron, P. Oliveira, L. Nadjo, Biomacromolecules 9 (2008) 812–817.
[11] C.V. Kumar, A. Buranaprapuk, J. Am. Chem. Soc. 121 (1999) 4262–4270.
[12] J.K. Choi, J. Ho, S. Curry, D. Qin, R. Bittman, J.A. Hamilton, J. Lipid Res. 43 (2002) 1000–1010.
[13] S. Makino, J.A. Reynolds, C. Tanford, J. Biol. Chem. 248 (1973) 4926–4932.
[14] Y. Zhang, D.E. Wilcox, J. Biol. Inorg. Chem. 7 (2002) 327–337.
[15] K. Kamikubo, S. Sakata, S. Nakamura, T. Komaki, K. Miura, J. Protein Chem. 9 (1990) 461–465.
[16] B. Sengupta, P.K. Sengupta, Biochem. Biophys. Res. Commun. 299 (2002) 400–403.
[17] X.Z. Feng, Z. Liu, L.J. Yang, C. Wang, C.L. Bai, Talanta 47 (1998) 1223–1229.
[18] J.C. D'Enon, A.J. Simpson, R. Kumar, A.J. Baer, S.A. Mabury, Environ. Toxicol. Chem. 29 (2010) 1678–1688.
[19] T. Peters, Adv. Protein Chem. 37 (1985) 161–245.
[20] T. Peters, All about albumin; biochemistry, Genetics and Medical Applications, Academic Press, New York, 1995.
[21] J.F. Foster, Albumin structure, Function and Uses, Pergamon Press, Oxford, UK, 1977.
[22] X.M. He, D.C. Carter, Nature 358 (1992) 209–215.
[23] N. Wang, L. Ye, F.F. Yan, R. Xu, Int. J. Pharm. 351 (2008) 55–60.
[24] D.C. Carter, J.X. Ho, Adv. Protein Chem. 45 (1994) 153–203.
[25] Y. Moriyama, D. Ohta, K. Hadiya, Y. Mitsui, K. Takeda, J. Protein Chem. 15 (1996) 265–272.
[26] A. Mallick, N. Chattopadhyay, Biophys. Chem. 109 (2004) 261–270.
[27] R.B. Singh, S. Mahanta, A. Bagchi, N. Guchhait, Photochem. Photobiol. Sci. 8 (2009) 101–110.
[28] R.B. Singh, S. Mahanta, N. Guchhait, J. Photochem. Photobiol. B 91 (2008) 1–8.
[29] A. Samanta, B.K. Paul, N. Guchhait, Biophys. Chem. 156 (2011) 128–139.
[30] O.K. Abou-Zied, O.I.K. Al-Shihi, J. Am. Chem. Soc. 130 (2008) 10793–10801.
[31] L. Painter, M.M. Harding, P.J. Beeby, J. Chem. Soc. Perkin Trans. 18 (1998) 3041–3044.
[32] M. Fischer, J. Georges, Chem. Phys. Lett. 260 (1996) 115–118.
[33] J.R. Lakowicz, Principles of Fluorescence Spectroscopy, Springer, New York, 2006.
[34] S.S. Lehrer, Biochemistry 10 (1971) 3254–3263.
[35] S. Sugio, A. Kashima, S. Mochizuki, M. Noda, K. Kobayashi, Protein Eng. 12 (1999) 439–446.
[36] M.J Frisch et al., Gaussian 03, Revision B.03, Gaussian, Inc., Pittsburgh, 2003.
[37] G.M. Morris, D.S. Goodsell, R.S. Halliday, R. Huey, W.E. Hart, R.K. Belew, A.J. Olson, J. Comput. Chem. 19 (1998) 1639–1662.
[38] S. Jana, S. Dalapati, S. Ghosh, N. Guchhait, J. Photochem. Photobiol. B 112 (2012) 48–58.
[39] P. Suppan, J. Chem. Soc. A (1968) 3125–3133.
[40] M. Belletête, R.S. Sarpal, G. Durocher, J. Phys. Chem. 99 (1995) 4015–4024.

[41] R.E. Maurice, A.G. Camillo, Anal. Biochem. 114 (1981) 199–212.
[42] P.D. Ross, S. Subramanian, Biochemistry 20 (1981) 3096–3102.
[43] T. Förster, Discuss. Faraday Soc. 27 (1959) 7–17.
[44] J.B.F. Lloyd, Nat. Phys. Sci. 231 (1971) 64–65.
[45] P. Yang, F. Gao, The Principle of Bioinorganic Chemistry, Science Press, 2002.
[46] K. Rahmelow, Anal. Biochem. 241 (1996) 5–10.
[47] S. Neelam, M. Gokara, B. Sudhamalla, D.G. Amooru, R. Subramanyam, J. Phys. Chem. B 114 (2010) 3005–3012.
[48] D.C. Carter, X.M. He, Science 249 (1990) 302–303.
[49] S. Jana, S. Ghosh, S. Dalapati, N. Guchhait, Photochem. Photobiol. Sci. 11 (2012) 323–332.